Biophysical Journal, Volume *112*

Supplemental Information

Structure and Intermolecular Interactions between *L*-Type Straight Flagellar Filaments

Daniel Louzon, Avi Ginsburg, Walter Schwenger, Tom Dvir, Zvonimir Dogic, and Uri Raviv

Structure and Intermolecular Interactions between L-type Straight Flagellar Filaments

D. Louzon, [*,†] A. Ginsburg, [*,‡] W. Schwenger, [§] T. Dvir, [*,†] Z. Dogic, [§] and U. Raviv [*]

[*] The Institute of Chemistry and the Center for Nanoscience and Nanotechnology, The Hebrew University of Jerusalem, Jerusalem, 91904, Israel. [†]The Racah Institute of Physics, The Hebrew University of Jerusalem, Jerusalem, 91904, Israel. [‡]The Institute for drug research, The Hebrew University of Jerusalem. [§] Department of Physics, Brandeis University, Waltham, MA 02454, USA.

SUPPORTING MATERIALS

1 Solvent subtraction

Fig. S1 shows that using Eq. 4 to subtract the displaced volume of the solvent did not improve the fit to our data. Hence Eq. 2 was used in subsequent models.

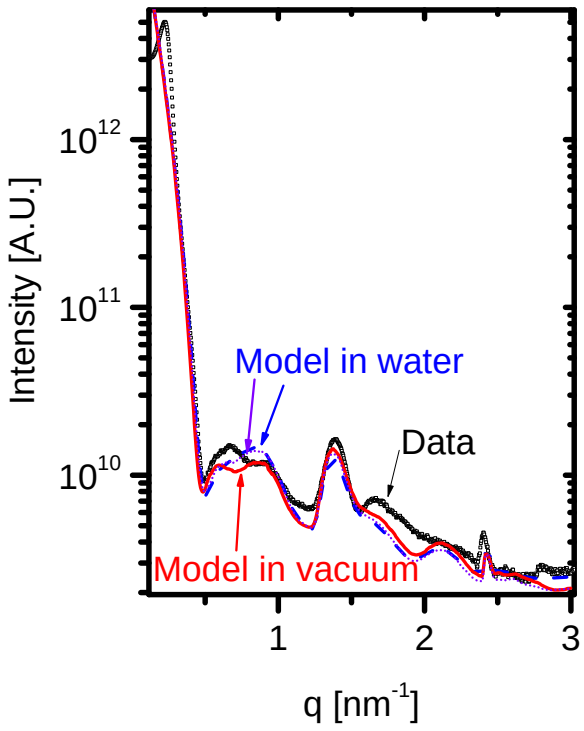

Figure S1: Radially integrated scattering intensity from SJW1660 strain (empty square symbols) and the computed form-factor of a flagella filament, averaged over all orientations in $\vec{q}$-space, using Eqs.2 and 7 (red solid curve) and after taking into account the contribution of the displaced solvent, using Eq. 7 and Eq. 4 with solvent mean electron density of $\rho_0 = 333\,{}^{e}/_{\mathrm{nm}^3}$ (blue broken curve) or with $\rho_0 = 303\,{}^{e}/_{\mathrm{nm}^3}$ (dotten violet curve).

© 2013 The Authors
0006-3495/08/09/2624/12 $2.00

2 Varying form-factor parameters

The flagella model (Fig. 3) is supported by the following considerations. The helical character of the structure is supported by looking at the aligned sample shown in Fig. 9. In this figure, the form factor features are governed by the helical shape of the filament at $q > 1\,\mathrm{nm}^{-1}$, indicating that the subunit packing must be considered in the form-factor model. Figs. S2-S4 show the high sensitivity of the calculated form-factor model to small changes in the helix diameter (Fig. S2), the helical pitch (Fig. S3), and the filament tilt angle (Fig. S4).

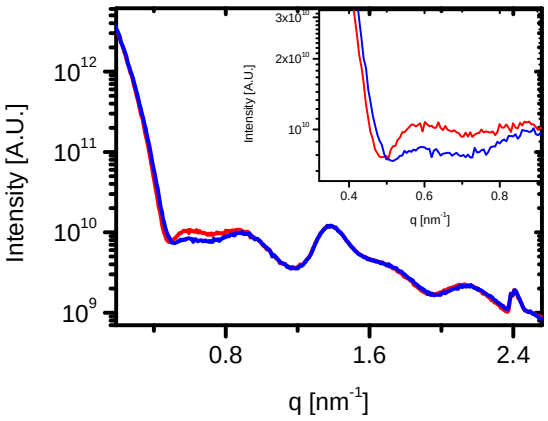

Figure S2: A comparison between two form-factor models with a $0.1\,\mathrm{nm}$ difference in the helix diameter. The main differences between the two models are the location of the first minimum and the amplitude of the following local maximum. The inset, shows these features on an expanded scale.

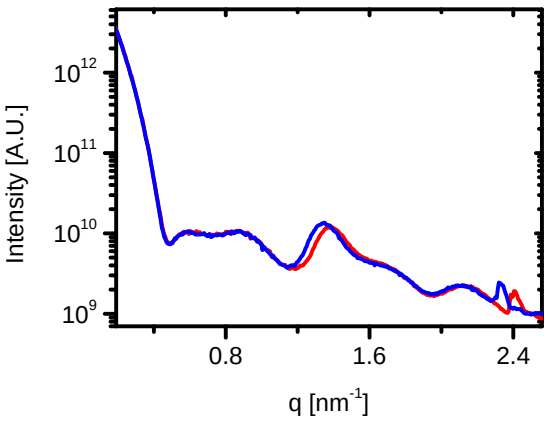

Figure S3: A comparison between two form-factor models with a $0.2\,\mathrm{nm}$ difference in the size of the two turn pitch. The main difference between the two models is the shift of the two layer-line peaks at $q \simeq 1.4\,\mathrm{nm}^{-1}$ and $q \simeq 2.4\,\mathrm{nm}^{-1}$.

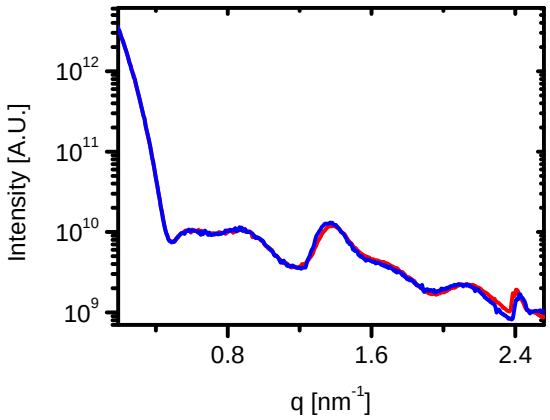

Figure S4: A comparison between two form-factor models with a 1° difference in the angle of the filament tilt. The tilt angle mainly changes the separation between the two layer-line peaks at $q \simeq 1.4\,\mathrm{nm}^{-1}$ and $q \simeq 2.4\,\mathrm{nm}^{-1}$.

Figs. S2-S4 clearly show that each of these parameters predominantly affects different features in the form-factor, allowing them to be optimized (or fit) independently. This fact increase our confidence level in the model.

Fig. S5 shows the calculated $I(q)$ derived from the model of flagellar filaments, arranged in a hexagonal lattice with no thermal fluctuations. The lattice-sum peaks dominates this model and there are almost no form-factor features at $q > \sim 0.5\,\mathrm{nm}^{-1}$.

3 Instrument resolution function

Fig. S5 shows that the intensity of the flagellar bundle model has sharp correlation peaks that were invisible in the SAXS results (Fig. 5). We attribute this observation to the resolution function of our measurement setups, defined by the monochromator, detector pixel size, beam size, sample-to-detector distance, etc. To account for these effects, each of the calculated model intensities was convoluted with a Gaussian function with a standard deviation, $\sigma = 0.03\,\mathrm{nm}^{-1}$, which is the measured resolution of our setup. Fig. S5 (red curve) shows that fewer measurable peaks are expected when the resolution function is taken into account.

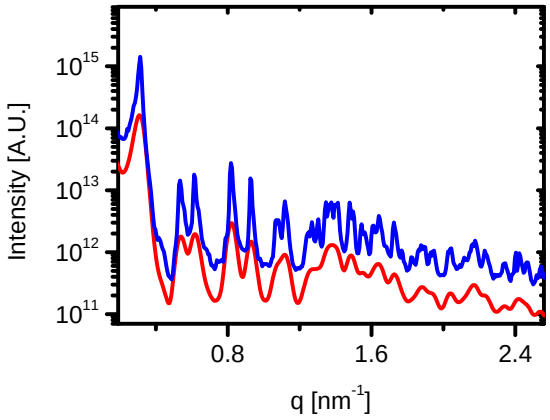

Figure S5: The calculated intensity (as a function of q) of a 15×15 bundle of filaments in a hexagonal lattice with no fluctuations(blue curve). The red curve results from the a convolution between the blue curve and a Gaussian resolution function with a standard deviation of $\sigma = 0.03\,\mathrm{nm}^{-1}$.

4 Varying Structure-factor parameters

The SAXS results (Fig. 5) show that both the structure factor peaks and the form-factor principle features can be observed. Fig. S6 compares between the calculated intensity models of flagellar filament hexagonal bundles with different degrees of thermal fluctuations. The extent of fluctuations was determined by the elastic constant between neighbours', κ, which determines the lattice-sum contribution to the calculated intensity. A sufficiently high κ value, significantly limits thermal fluctuations and the intensity resembles the calculated intensity assuming no thermal fluctuations (Fig. S5, blue curve). If, however, the value of κ is too low, the hexagonal lattice is unstable and the lattice-sum peaks become unclear (Fig. S6, blue curve).

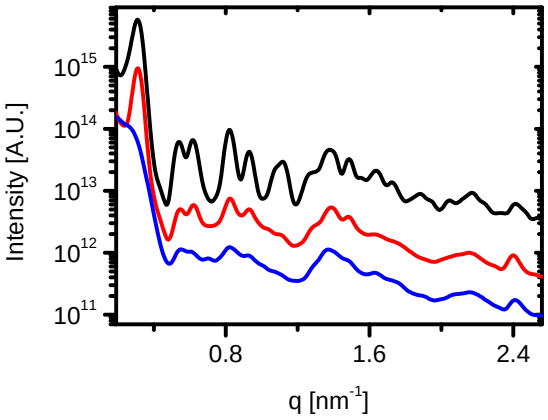

Figure S6: A comparison between the lattice sum contribution to the calculated intensity of three models with different κ values. $\kappa = 8\,\mathrm{mN}\cdot\mathrm{m}^{-1}$ (black curve), $\kappa = 0.8\,\mathrm{mN}\cdot\mathrm{m}^{-1}$ (red curve), and $\kappa = 0.08\,\mathrm{mN}\cdot\mathrm{m}^{-1}$ (blue curve).

The hexagonal lattice constant, a, affects the location of the peaks in the calculated intensity. Fig. S7 shows models with a small difference in the value of a. The figure clearly shows that the model is very sensitive to the value of a, hence a can be accurately determined.

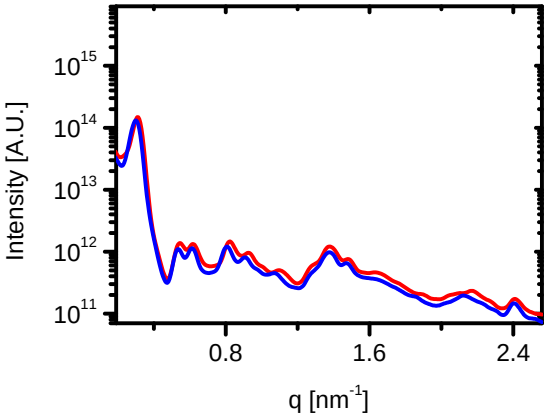

Figure S7: A comparison between the calculated scattering intensities of two models of bundles with a small difference in their lattice constants. The blue curve is with $a = 23.4\,\mathrm{nm}$ and the red curve with $a = 23.8\,\mathrm{nm}$. As the lattice constant increases the correlation peaks shift to lower q values.

Fig. 8 shows how the calculated intensity, $I(q)$, is affected by the size of the bundle. Here the main feature that is affected is the width of the peaks. To clearly see that, the results before and after applying the convolution with the experimental resolution function are shown.

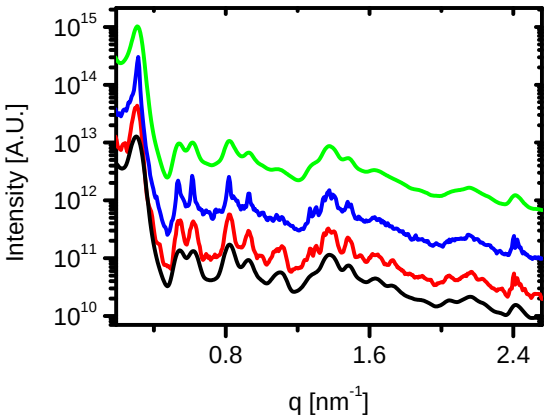

Figure S8: A comparison between the calculated intensity of two models with different sizes of bundles. The red curve corresponds to a bundle of 6×6. The blue curve corresponds to a bundle of 15×15. The difference in the width of the peaks is less clear after applying the resolution function (black for the 6×6 bundle and green for the 15×15 bundle) Note that after applying the resolution function, in the smaller bundle model the peaks at high q and are more distinct.

Unlike the form-factor parameters, the lattice-sum parameters are more dependent of each other and it is possible to attain similar fits by fine tuning κ or the bundle size. These parameters should therefore be considered more carefully. It is, however, clear that the model provides the correct order of magnitude of these parameters.

5 Osmotic stress experiments

Fig. S9 provides additional SAXS curves from flagellar bundles formed under different osmotic pressures, as in Fig. 5.

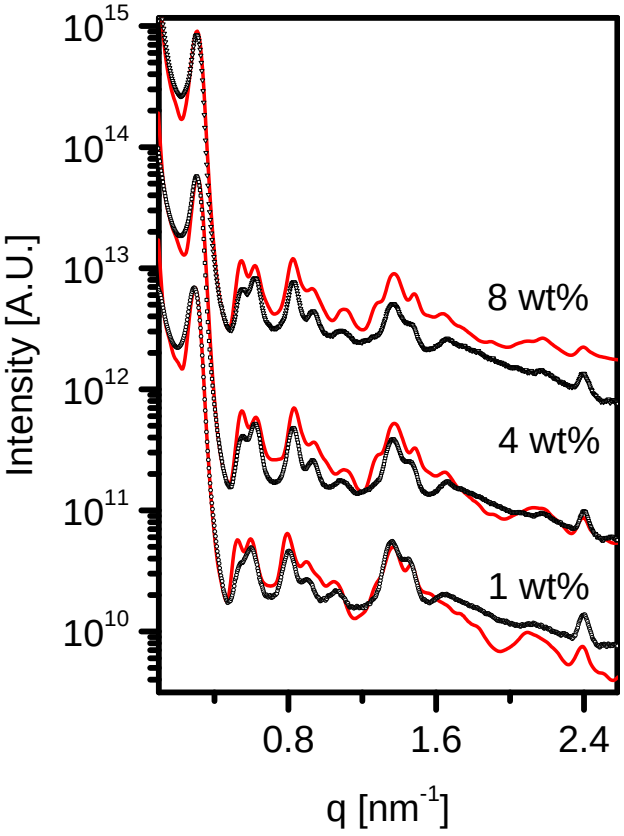

Figure S9: Additional SAXS measurements of SJW1660 in 100 mM NaCl and 10 mM K_2HPO_4 under different PEG ($M_w = 20,000$ Da) concentrations (in wt%), as indicated (black symbols) with the corresponding computed models (red curve).

6 Equation of state

The equation-of-states for a bundle of long semi-flexible chains in solution is:

$$\frac{\partial G}{\partial d}(d) = \frac{\partial H_0}{\partial d}(d) + ck_BT\kappa_s^{-\frac{1}{4}}\frac{\partial}{\partial d}\sqrt[4]{\frac{\partial^2 H_0}{\partial d^2}} \tag{1}$$

where G is the free energy, $d = a - D$ is the spacing between filaments, κ_s is the bending stiffness, H_0 is:

$$H_0(d) = a_h\frac{e^{-d/\lambda_H}}{\sqrt{d/\lambda_H}} + b\frac{e^{-d/\lambda_D}}{\sqrt{d/\lambda_D}}, \tag{2}$$

where λ_H and λ_D are the hydration and electrostatic screening lengths. The first derivative of H_0 is:

$$\frac{\partial H_0}{\partial d}(d) = -\frac{a_h\left(\frac{2d}{\lambda_H}+1\right)\mathrm{e}^{-\frac{d}{\lambda_H}}}{2\lambda_H\left(\frac{d}{\lambda_H}\right)^{\frac{3}{2}}} - \frac{b\left(\frac{2d}{\lambda_D}+1\right)\mathrm{e}^{-\frac{d}{\lambda_D}}}{2\lambda_D\left(\frac{d}{\lambda_D}\right)^{\frac{3}{2}}} \tag{3}$$

and its second derivative is:

$$\frac{\partial^2 H_0}{\partial d^2}(d) = \frac{a_h\left(\frac{4d^2}{\lambda_H}+4d+3\lambda_H\right)\mathrm{e}^{-\frac{d}{\lambda_H}}}{4\lambda_H^3\left(\frac{d}{\lambda_H}\right)^{\frac{5}{2}}} + \frac{b\left(\frac{4d^2}{\lambda_D}+4d+3\lambda_D\right)\mathrm{e}^{-\frac{d}{\lambda_D}}}{4\lambda_D^3\left(\frac{d}{\lambda_D}\right)^{\frac{5}{2}}} \tag{4}$$

The last term of the equation of state is then:

$$\frac{\partial}{\partial d}\sqrt[4]{\frac{\partial^2 H_0}{\partial d^2}} = -\frac{(\alpha+\beta)\,\mathrm{e}^{-\frac{d}{\lambda_H}-\frac{d}{\lambda_D}}}{\gamma} \tag{5}$$

where

$$\alpha = \left(\frac{d}{\lambda_H}\right)^{\frac{7}{2}}\left(8b\lambda_H^6 d^3 + 12b\lambda_D\lambda_H^6 d^2 + 18b\lambda_D^2\lambda_H^6 x + 15b\lambda_D^3\lambda_H^6\right)\mathrm{e}^{\frac{d}{\lambda_H}} \tag{6}$$

$$\beta = \left(\frac{d}{\lambda_D}\right)^{\frac{7}{2}}\left(8a\lambda_D^6 d^3 + 12a_h\lambda_D^6\lambda_H d^2 + 18a_h\lambda_D^6\lambda_H^2 d + 15a_h\lambda_D^6\lambda_H^3\right)\mathrm{e}^{\frac{d}{\lambda_D}} \tag{7}$$

and

$$\gamma = 32\lambda_D^6\lambda_H^6\left(\frac{d}{\lambda_D}\right)^{\frac{7}{2}}\left(\frac{d}{l}\right)^{\frac{7}{2}}\left(\frac{a_h\left(\frac{4d^2}{\lambda_H}+4d+3\lambda_H\right)\mathrm{e}^{-\frac{d}{\lambda_H}}}{4\lambda_H^3\left(\frac{d}{\lambda_H}\right)^{\frac{5}{2}}} + \frac{b\left(\frac{4d^2}{\lambda_D}+4d+3\lambda_D\right)\mathrm{e}^{-\frac{d}{\lambda_D}}}{4\lambda_D^3\left(\frac{d}{\lambda_D}\right)^{\frac{5}{2}}}\right)^{\frac{3}{4}} \tag{8}$$

In a hexagonal lattice, the relation between the free energy and the osmotic pressure is:

$$-\frac{\partial G}{\partial d}(d) = \sqrt{3}\Pi d. \tag{9}$$